Telephone cord buckles-A relation between wavelength and adhesion

Jean-Yvon Faou, Guillaume Parry, Sergey Grachev, Etienne Barthel

Telephone cord buckles – a relation between wavelength and adhesion

Jean-Yvon Faou[a], Guillaume Parry[b,c], Sergey Grachev[a], Etienne Barthel[d,e1]

[a] *Surface du Verre et Interfaces, UMR 125 CNRS/Saint-Gobain, 39 Quai Lucien Lefranc, F-93303 Aubervilliers, Cedex, France.*

[b] *Univ. Grenoble Alpes, SIMAP, F-38000 Grenoble, France.*

[c] *CNRS, SIMAP, F-38000 Grenoble, France.*

[d] *École Supérieure de Physique et de Chimie Industrielles de la Ville de Paris (ESPCI) ParisTech, PSL Research University, Sciences et Ingénierie de la matière Molle, CNRS UMR 7615, 10, Rue Vauquelin, F-75231 Paris Cedex 05, France.*

[e] *Sorbonne-Universités, UPMC Univ. Paris 06, SIMM, 10, Rue Vauquelin, F-75231 Paris Cedex 05, France.*

Abstract

Thin films with low adhesion and large residual stresses may buckle. The resulting morphologies are varied, but one of the most commonly observed is an intriguing oscillating pattern – the so-called "telephone cord" – which has been extensively investigated in the recent years. We have studied the kinematics of formation of telephone cords using a geometrically non-linear plate model and mode dependent interfacial toughness, captured *via* a cohesive zone. Through extensive Finite Element Simulations, we have demonstrated a simple, non trivial relation between telephone cord wavelength and interfacial toughness. To validate this prediction, highly stressed Mo thin films where deposited on Si wafers, with a well defined interface and very reproducible adhesion. Studying the morphology of the resulting buckles for different film thicknesses and stresses, we observed a trend which was fully consistent with our simulation results. From the data fit, an adhesion energy of $0.58 \pm 0.04\,\mathrm{Jm}^{-2}$ for the SiO_2/Ag interface was inferred, which compares well with literature estimates.

[1]Corresponding author. Email address: etienne.barthel@saint-gobain.com

1. Introduction

Coatings are widely used for surface functionalization so that the mechanical stability of coatings is of critical importance in many applications. An elastic film subject to in-plane compression may partially delaminate and form blisters (Fig. 1) depending on factors such as thickness, stress and adhesion. Indeed buckling driven delamination is a frequent failure mode when the coating is subject to external or residual compressive stresses and adhesion is low. This subject has been investigated for many years and a variety of blister morphologies have been studied (Gilles and Rau, 1984; Wang and Evans, 1999; Thouless, 1993; Evans and Hutchinson, 1984; Hutchinson, 2001; Moon et al., 2004; Yu et al., 2013).

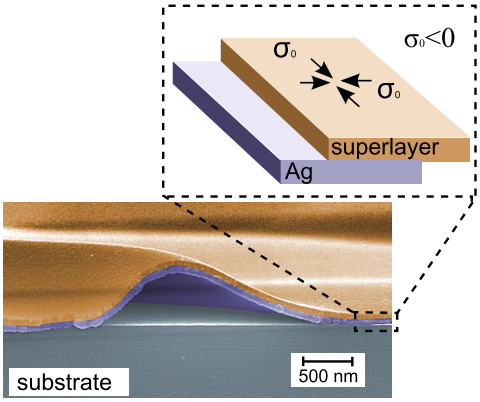

Figure 1: Scanning electron micrograph of a buckled thin film (cross-section). The stack consists of 80 nm of molybdenum and 80 nm of silver on a silicon wafer.

The problem is to couple plate non-linearity with adhesion. For simple buckle morphologies such as straight sided and circular blisters, relations between buckle size and adhesion have been obtained (Hutchinson and Suo, 1992a; Hutchinson et al., 1992b; Jensen, 1993). From these relations one would be able to derive film adhesion from the measurement of the buckle width (straight sided) or buckle diameter (circular). Unfortunately both straight and circular blisters are seldom found in practice. In the ubiquitous case of equi-biaxial compression, by far the most usual morphology is an undulating blister called telephone cord (TC) buckle (Moon et al., 2002a). However, the morphology of TCs is poorly understood. As an approximation, it was proposed to map the buckle morphology to simpler blister geometries, namely a circular or a pinned circular blister (Moon et al., 2002b). With

this method the energy release rate can be estimated from the width of the blister (Cordill et al., 2007; Lee et al., 2005). Along a different route, Gioia and Ortiz (1998) have proposed an approximate plate theory to model the morphology of undulating buckles, from which they derived a relation between adhesion and TC buckle period. However, these methods rely on approximate descriptions so that, to date, no clear relation between adhesion and morphological parameters of TC buckles is available.

In a previous work, we have explored the kinematics of TC propagation and demonstrated how it results in the TC morphology: mode dependent adhesion conspires with local sagging of the film to form effective pinning points, from which the oscillating propagation of TCs results (Faou et al., 2012). Here we present a more quantitative investigation of the impact of TC formation kinematics on morphology. Rationalizing the morphologies of simulated buckles for various film thicknesses, residual stresses and adhesion, we find an unexpectedly simple relation between TC *wavelength* (not width) and adhesion. To test this prediction, we have studied the morphology of a variety of Mo buckles with different thicknesses and stresses and constant adhesion. We find that a reasonable value of film adhesion can indeed be derived from this relation, which compares favorably with literature values.

2. Previous results

We first summarize previous results concerning the relations between blister geometry, loading and adhesion. We consider an elastic film with Young's modulus E, Poisson's ratio ν, thickness h, in-plane equi-biaxial compressive stress σ_0 and adhesion (or rather interfacial toughness) G_c.

2.1. Straight sided blisters

Although straight sided delamination is rarely observed, we briefly summarize the main results here to introduce the key concepts. Hutchinson and Suo (1992a) modeled the straight sided blister as a clamped Euler column. Bending of thin plates is described by the non-linear Foppl-Von Kármán equations. For a straight sided blister the strain component along the blister direction is unaffected by buckling whereas the stress is partially relaxed in the perpendicular direction. It is found that the blister profile is sinusoidal. Denoting $2b$ the blister width, the critical buckling stress σ_c for buckling is

given by

$$\sigma_c = \frac{\pi^2}{12}\frac{E}{1-\nu^2}\left(\frac{h}{b}\right)^2 \tag{1}$$

For a straight sided blister, the loading ratio σ_0/σ_c is the sole parameter governing the buckle shape. For instance the buckle height is

$$\frac{\delta}{h} = \sqrt{\frac{4}{3}\left(\frac{\sigma_0}{\sigma_c} - 1\right)}$$

a form which highlights the non linearity of the problem. Similarly the energy release rate depends only on the loading ratio.

Adhesion is introduced when this solution is coupled to an edge crack. The total elastic energy stored in the film is $G_0 = ((1-\nu)/E)\sigma_0^2 h$. A fraction of this energy can be released during crack propagation to overcome adhesion. But this energy release rate G is mainly an increasing function of the width $2b$ so that in this simpler picture, it is expected that buckles are unstable. However it has been evidenced experimentally (Liechti and Chai, 1992) that crack face separation in shear (mode II) requires more energy than pure opening (mode I). Hutchinson and Suo (1992a) pointed out that as the straight sided buckles becomes wider, the shear contribution increases, so that G_c may eventually reach G whereupon the edge crack stops.

In brief, in the buckle problem, the main stabilizing force is provided by the mode dependence of interfacial toughness so that the morphology results from the interplay between plate geometric non-linearities and mode dependent adhesion.

2.2. Telephone cord blisters

Unlike the straight sided blister, undulating patterns such as TCs partially relax film stresses along both transverse *and* axial directions. As a result, the energy release rate G is larger.

In their detailed investigation of TC morphologies, Moon et al. (2004) pointed out that the precise experimental determination of TC width $2b$ is by itself a complex problem, as several candidate measures arise. In practice $2b$ is often defined as the width within which the TC buckle is confined (Moon et al., 2004). Besides the width, they also focussed on the wavelength λ and drew two conclusions about the *aspect ratio* $\lambda/2b$: 1) the aspect ratio is *not* a constant, but varies from about 0.8 to 1.5; 2) the aspect ratio is *not* a function of the loading ratio σ_0/σ_c only.

In an attempt to better understand the wavelength, Moon et al. (2002b) built upon the idea of secondary buckling. Indeed the TC morphology can be approximately reproduced assuming that there is no adhesion over a strip of width $2b$: when the loading ratio exceeds $\sigma_0/\sigma_c = 6.5$ (Audoly , 1999; Audoly et al., 2002; Parry et al., 2006) (for $\nu = 0.3$) the plate destabilizes from straight sided into wavy bukles, a morphology quite similar to TCs. However, using Finite Element Analysis of these wavy buckles, Moon et al. (2004) found that the energy release rate is *independent* of the wavelength. In brief, secondary buckling *does not* predict the aspect ratio.

3. FEM model for buckling driven delamination

To analyze the morphology of TC buckles, we use our recent model, which has been briefly described earlier (Faou et al., 2012). The thin film is modeled as a geometrically non-linear plate, as depicted in Fig. 2. The midplane surface is defined by the (O, x, y) plane, with (u, v, w) the respective displacement components along the axes (Ox, Oy, Oz) for any point of the midplane. The various buckling patterns are characterized by large values of the out-of-plane displacement $w(x, y)$, and the calculation must be carried out within the framework of large displacements using the Green Lagrange strain tensor.

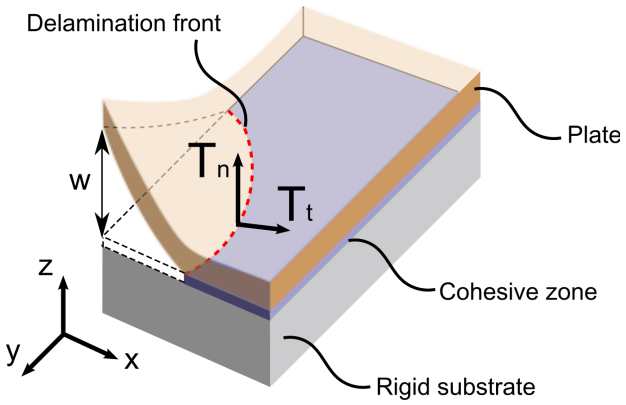

Figure 2: Schematic sketch of the model.

3.1. Modeling of the film/substrate interface

For the interface debonding process, a mixed-mode cohesive zone model is used. Cohesive zone models have been widely used and implemented for frac-

ture mechanics studies for the last two decades (Tvergaard and Hutchinson, 1992; Xu and Needleman, 1993; Barthel, 1998). The constitutive behavior of the interface consists of a traction vs. separation law. Due to interaction between the two separating faces, the interface traction $\overline{T}$ depends upon the separation vector $\overline{\delta}$, which is the relative displacement between opposite crack faces at a point initially joined on the interface. The separation and traction vectors can be resolved into their normal components (δ_n, T_n), the opening or mode I contribution, and their tangential components resolved in the direction normal to the crack front, (δ_t, T_t), the shearing or mode II contribution. The tangential component resolved tangent to the crack front, the mode III contribution, is not expected to play an important role and is not taken into account in the traction-separation law.

As described in the previous section, an essential aspect of the buckling delamination phenomenon is mixed mode behavior with higher resistance to delamination under mode II than mode I. The following mixed mode traction-separation law embodies this type of dependency, and it can be implemented as a standard ABAQUS cohesive element (COH) (ABAQUS, 2010). The law is a linear/softening model depicted in Fig. 3. In Stage 1, prior to attaining the peak traction, the traction-separation relation is linear and reversible:

$$\overline{T} = K\overline{\delta} \tag{2}$$

with stiffness K. For any combination of traction components, (T_n, T_t), peak values $({T_n}^i, {T_t}^i)$ are reached when (c.f., Fig. 3)

$$\left(\frac{T_n}{{T_n}^0}\right)^2 + \left(\frac{T_t}{T_t^0}\right)^2 = 1 \tag{3}$$

where T_n^0 is the maximum traction in mode I and T_t^0 is the maximum traction in mode II. The corresponding separations at the peak are $\overline{\delta^i} = (\delta_n^i, \delta_t^i)$. Once peak traction is attained, softening sets in (Stage 2), resulting in decreasing traction, as in Fig. 3.

The two stages are combined such that the separation energy/area, $G_c(\psi)$, depends on the mode mix ψ in a specific manner, as now described. The measure of the mode mix in the cohesive law is defined in terms of the combination of tractions attained at the peak, as the angle where $\tan(\psi) = T_t^i/T_n^i$. This definition differs from that employed in linear fracture mechanics in that it is defined point-wise on the interface in the vicinity of crack front (i.e., from element to element), whereas the conventional definition of mode

mix, ψ, is defined in terms of the mode I and II stress intensity factors at the crack front as $\tan(\psi) = K_{II}/K_I$. The definition of ψ used here is natural within the context of a cohesive law employed in a numerical finite element simulation wherein a softening traction behavior is assigned for the remaining interface resistance after the peak is attained in a manner depending on the mode experienced at that point on the interface.

The separation energy/area, $G_c(\psi)$, is taken to have a dependence on mode mix characterized by the relation

$$G_c(\psi) = G_{Ic}(1 + \tan^2(\eta\psi)) \tag{4}$$

with G_{Ic} as the mode I separation energy, or toughness, and a dependence on the parameter η seen in Fig. 4. This is a phenomenological relation that has been successfully fit to experimental data sets for various interfaces (Hutchinson and Suo, 1992a). Values of η close to zero imply a weak dependence on the mode mix, while values close to unity have a strong dependence. With Eq. 4

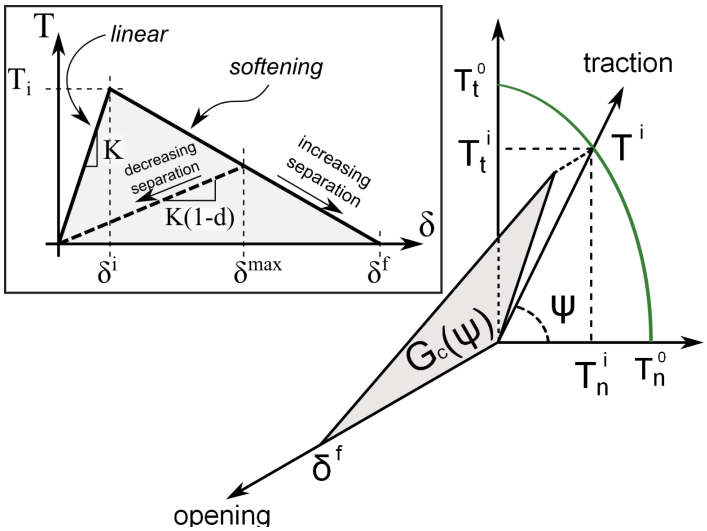

Figure 3: Traction vs separation law for interfacial toughness at the film/substrate interface including mixed mode dependence. Inset: schematic of the linear/softening traction separation law, in one dimension, also showing interfacial toughness as the total work done by the cohesive stress upon complete opening of the cohesive element (shaded area).

as the total separation energy and ψ determined by the traction combination attained at the peak, a (scalar) effective relative interface displacement at

complete separation δ^f is defined from the relation

$$G_c(\psi) = \frac{1}{2}\delta^f T^i \tag{5}$$

where $T^i = \sqrt{T_n^{i\,2} + T_t^{i\,2}}$ is the peak stress magnitude. The softening is implemented as a reduction of the stiffness by the factor $(1-d)$ where d can be regarded as a damage variable. The definition of the cohesive traction Eq. 2 becomes

$$\overline{T} = K(1-d)\overline{\delta} \tag{6}$$

The variable d is defined as

$$d = \frac{\delta^f}{\delta}\frac{\delta - \delta^i}{\delta^f - \delta^i} \tag{7}$$

where δ is the separation magnitude

$$\delta = \sqrt{\delta_n^2 + \delta_t^2} \tag{8}$$

and similarly δ^i is the peak separation magnitude. Inserting Eq. 7 into Eq. 6 we obtain

$$\overline{T} = T^i \frac{\delta^f - \delta}{\delta^f - \delta^i}\frac{\overline{\delta}}{\delta} \tag{9}$$

which shows that $\overline{T}$, which is colinear with the current separation $\overline{\delta}$, has a magnitude proportionally reduced from T^i. Integration of the work of the cohesive tractions using Eq. 2 in Stage 1 to (T_n^i, T_t^i) and then, in Stage 2, to full separation using Eq. 9 gives $1/2\delta^f T^i$. Thus, the definition of δ^f in Eq. 5 provides the desired mode-dependent separation energy.

In the simulations of buckling delamination some regions of the crack front are observed to undergo softening separations beyond the peak and then, prior to complete separation, the separation reverses, or unloads, as depicted in Fig. 3. Beyond the peak, we assume that the interface has undergone irreversible damage and the unloading response is a linear connection to the origin of the traction-separation relation (Fig. 3), as results when in Eq. 7 δ is fixed at the maximum value attained δ_{max}.

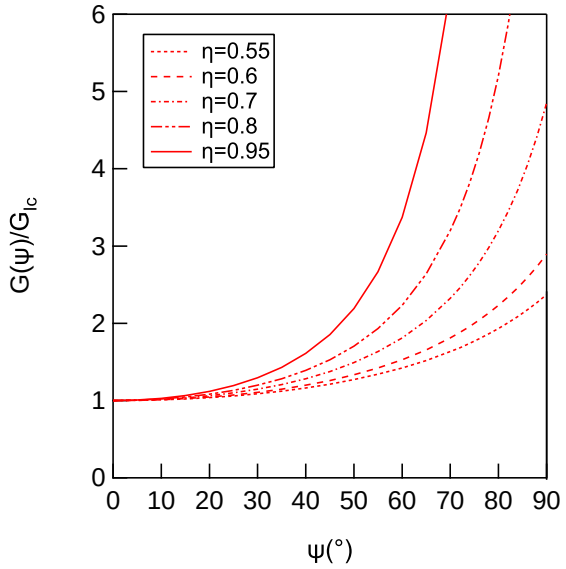

Figure 4: Mode dependence of interfacial toughness, plotted from Eq. 4. The amplitude is directly set by the mode mixity parameter η.

3.2. Loading and boundary conditions

The loading consists of an eigenstrain $\epsilon_0 > 0$ applied uniformly to the plate ($\epsilon_{xx} = \epsilon_{yy} = \epsilon_0$, $\epsilon_{xy} = 0$) at time $t = 0$. An equi-biaxial compressive stress state is generated in the flat adherent parts of the film: $\sigma_{xx} = \sigma_{yy} = -E/(1-\nu)\epsilon_0 = -\sigma_0$, $\sigma_{xy} = 0$.

Nucleation is controlled with a small rectangular strip located near an edge of the domain. This area remains adhesion-free so that it can buckle and nucleate a delamination front that will subsequently propagate along the plate-substrate interface.

The calculations are carried out with the Finite Element Method, using the software ABAQUS (ABAQUS, 2010). Triangular shell elements are used for the film, within a large displacement framework. The element size is chosen so that there are about 40 elements in the buckle width. Quadrilateral cohesive elements are used in order to model the interface behavior. The upper surface is tied to the shell elements, whereas the lower surface is fixed since the substrate is rigid (Fig. 2). Because during subsequent evolution of the plate, the gap may close back after cohesive elements have been broken, a unilateral contact condition $w(x, y) \geq 0$ is added to the shell elements. It is not implemented in the cohesive element, but is managed separately using

a classical hard/frictionless contact algorithm. With this unilateral contact conditions plate-substrate interpenetration is avoided.

A quasi-static analysis is carried out using the explicit solver of ABAQUS. Due to the presence of two sources of non-linearity (geometrical non-linearity and cohesive law), an explicit algorithm is more efficient even if the analysis is quasi-static. This approach is commonly adopted, requiring the dynamic parameters to be chosen carefully so that the kinetic energy always remains very small compared to the strain energy in the elements. A number of implicit calculations have also been carried out and very good agreement with explicit results is obtained.

For all simulations, Poisson's ratio was kept equal to 0.31 and a strong mode II dependence was chosen with $\eta = 0.95$. K is chosen so that $\delta^i \ll \delta^f$, while T_n^0=17 MPa and T_t^0=200 MPa.

It would have been useful to choose the variable simulation parameters so as to keep the loading ratio σ_0/σ_c constant but it cannot be estimated prior to the simulation since the width $2b$ is a result of the calculations. More directly, material parameters were varied according to two normalized ratios. $\sigma_0/\bar{E}$ was varied from 1×10^{-3} to 1×10^{-2} and G_0/G_{Ic} from 0.1 to 0.6.

4. Numerical results

The results evidence a wide variety of morphologies (Fig. 5).

4.1. Relation between loading ratio and aspect ratio

Following Moon et al. (2004) we have inspected the aspect ratio and found values ranging from $\lambda/2b = 0.8$ up to $\lambda/2b = 1.5$. We have also evaluated the loading ratio σ_0/σ_c from Eq. 1 taking the full width of the TC buckle for $2b$ (Fig. 5). Loading ratios *vs.* aspect ratios are plotted in Fig. 6 left. A dispersion similar to Moon et al. (2004) is observed.

To go further, we color-coded the simulation points with the energy ratio G_0/G_{Ic} and found that smaller values of energy ratio correlate with larger aspect ratios. In fact iso-values of energy ratio define a family of parallel curves. We also found that normalizing the loading ratio by $\sqrt{\frac{G_0}{G_{Ic}} - 1}$ collapses all the points on a single master curve (Fig. 6 right). This *normalized loading ratio* is now a strictly decreasing function of the aspect ratio.

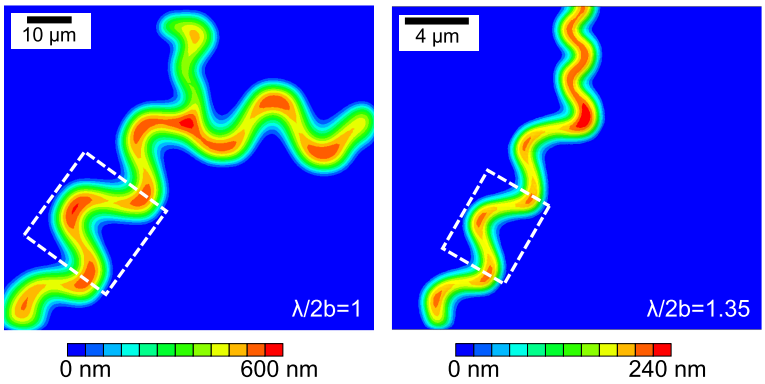

Figure 5: Out of plane displacement for two different TC morphologies obtained by numerical simulations, with $E = 329$ GPa: (left) $h = 100$ nm, $\sigma_0 = 2.5$ GPa, $G_{Ic} = 0.477$ J.m^{-2} resulting in an aspect ration of 1.0; (right) $h = 40$ nm, $\sigma_0 = 3.1$ GPa, $G_{Ic} = 0.4$ J.m^{-2} with an aspect ratio 1.35.

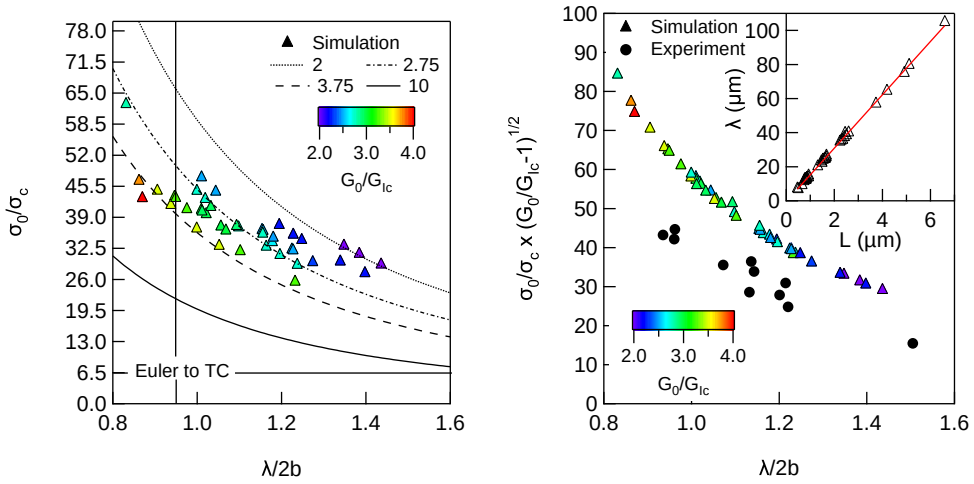

Figure 6: Numerical results: (left) loading ratio σ_0/σ_c as a function of the aspect ratio $\lambda/2b$, color coded with G_0/G_{Ic}. Also shown is the critical loading ratio at which the transition from straight sided (Euler) to wavy (TC) buckle is expected to occur from linear stability analysis (Audoly , 1999), and the expected wavelength; (right) normalized loading ratio (Eq. 10) as a function of aspect ratio, and resulting linear relation for λ (inset, Eq. 11). The dots are experimental data points from section 5.

4.2. Wavelength of the delamination pattern

Fitting the master curve connecting aspect ratio and normalized loading ratio gives a quadratic relation

$$\frac{\sigma_0}{\sigma_c}\sqrt{\frac{G_0}{G_{Ic}}-1} \propto \left(\frac{2b}{\lambda}\right)^2 \tag{10}$$

Since the loading ratio itself depends quadratically upon the width $2b$ through Eq. 1, the width actually drops out of Eq. 10. As a result we find that the quantity which is directly linked to interfacial toughness is the *wavelength* of the TC buckle, not the width. In summary the relation between λ and interfacial toughness can be expressed as:

$$\lambda = kL = kh\sqrt{\frac{E}{\sigma_0}}\left(\frac{G_0}{G_{Ic}} - 1\right)^{-1/4} \tag{11}$$

where all the other variables are in fact known material parameters or geometrical quantities. Relation 11 is plotted in Fig. 6 (right, inset). The slope $k = 14.5$.

5. Experiments - Relation between wavelength and adhesion

With Eq. 11 we can consider measuring adhesion from buckle wavelength. To experiment on the morphologies of TC buckles and test this prediction, we turned to the well calibrated two-layer thin films we have used previously (Faou et al., 2012). In this system a 15nm thick silver layer is deposited onto the native oxide of a two-inch (1 0 0) oriented silicon wafer. A cap layer of compressively stressed molybdenum is added to provide elastic energy for buckling driven delamination. The sample structure is illustrated in Fig. 1, where the Ag layer is a much thicker than usual for clarity.

5.1. Interface formation and thin film deposition

The films are sputtered in a high vacuum sputter deposition chamber equipped with two DC magnetron sputtering guns. Argon was used as the sputtering gas for both silver and molybdenum. Molybdenum thin films were sputtered at 2×10^{-6} bar of Ar, lowest pressure for which stable plasma could be maintained. Film stresses were measured in-situ by curvature measurement for each sample. A detailed study of residual stress tuning can be found in a previous publication (Faou et al., 2013). In brief, low deposition pressure results in high compression in molybdenum thin films. This is due to the large mean free path of argon neutrals, thus enhancing energies at which they bombard the sample. Higher energies result in atomic peening, causing compressive stress. Another smaller contribution to the compressive stress is ion peening. It remains small due to the low number of ionized species reaching the sample. The contribution can be enhanced by accelerating positive ions with the help of negative bias on the sample. Control over the

negative bias provides a good command of the residual compressive stress in the molybdenum top layer.

Deposition time for molybdenum ranges from 3 to 8 minutes resulting in film thickness 80 to 180 nm having a residual compression between 1.7 and 2.3 GPa in equi-biaxial state.

Delamination was observed when the sample was brought to atmospheric pressure. Direct observation of the interface separation was made under scanning electron microscope. For all samples, delamination occurred at the interface between the native oxide of the substrate and silver (Fig. 1). The topography of the buckles was determined by atomic force microscopy. As the wavelength is very sensitive to adhesion, the λ values are averages over ten periods. The width $2b$ is the total width within which the buckle is contained.

We observed TC buckles for $0.89 < G_0 < 1.5$ J.m^{-2}. TCs do not form if the elastic energy per unit area is too small compared to adhesion, and if it is too large, the film completely delaminates without forming TC patterns. Three examples of TCs with different morphologies are presented in Fig. 7. Morphological parameters and mechanical loading for all the buckles are

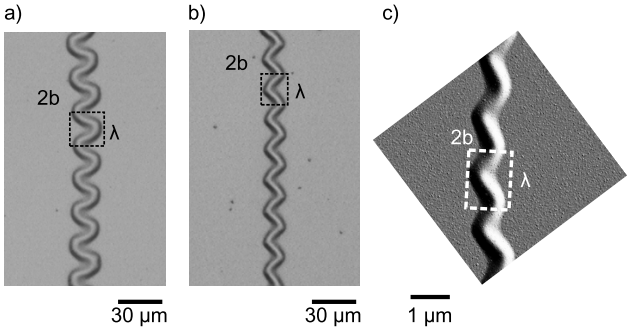

Figure 7: Microscopy photographs (a,b) and AFM phase image (c) for different values of G_0 for the same interface, and hence same adhesion G_1^c. This series of images illustrate the variation of the aspect ratio $\lambda/2b$ with G_0/G_1^c.

summarized in Table 1.

5.2. Experimental relation between loading ratio and aspect ratio

The aspect ratios $\lambda/2b$ of the TC buckles we have obtained range from 0.8 to 1.5, which is similar to the observations reported by Moon et al. (2004) and to the values obtained in the previous section. The loading ratio σ_0/σ_c

Table 1: Experiments: thickness, in-plane residual stress, wavelength of the TC blister, total elastic energy for Mo films on Ag/SiO_2 interface.

h (nm)	σ_0 (GPa)	λ (μm)	$2b$ (μm)	G_0 (J/m^2)
25	4.00	3.1	2.1	0.84
81	2.29	14.4	12.6	0.89
94	2.15	17.5	15.4	0.91
95	2.06	17.8	16.6	0.85
101	2.25	16.4	13.5	1.08
106	2.34	14.4	15.4	1.22
108	1.98	19.4	20.2	0.89
120	1.72	27.9	29.0	0.74
137	1.81	24.0	21.2	0.94
156	2.10	20.5	16.8	1.44
177	1.74	29.9	24.9	1.12

calculated from residual stress and total width (Eq. 1 and Table 1) is plotted against aspect ratio $\lambda/2b$ in Fig. 8.

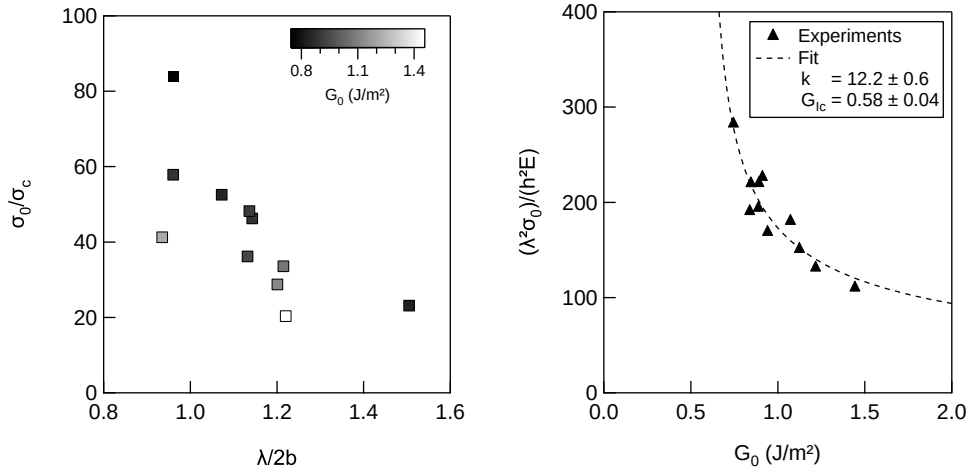

Figure 8: (left) measured loading ratio σ_0/σ_c as a function of aspect ratio $\lambda/2b$ for a series of films with identical SiO_2/Ag interface; (right) non-dimensional loading parameter for the experimental TC buckle as a function of total elastic energy prior rupture.

We observe a general trend for the loading ratio to decrease as aspect ratio increases but there is a significant dispersion, similar to Moon et al. (2004)'s. However, color coding the points with elastic energy stored in the

film (Fig. 8) suggests that the results can indeed be rationalized following Eq. 10. To do so, we need to identify the optimal value of interfacial toughness G_{Ic} for the SiO_2/Ag interface. Equivalently, this can be done by a least square fit based on Eq. 11 with G_{Ic} and k as free variables. In Fig. 8 we plot the non-dimensional loading parameter $(\lambda/h)^2\sigma/E$ as a function of the total elastic energy in the film G_0 along with the best fit ($k = 12.3 \pm 0.6$ and $G_{Ic} = 0.58 \pm 0.04\ \mathrm{Jm}^{-2}$). This value of mode I interfacial toughness is consistent with the values measured by cleavage test (0.8 Jm^{-2} (Barthel et al., 2005) and 0.5 Jm^{-2} (Patinet et al., 2013) for oxidized Si_3N_4/Ag). Using this value for G_{Ic} we also plotted the data on Fig. 6.

6. Discussion

6.1. Kinematics and wavelength

Dimensional analysis of the Von Karman plate equations for in-plane compressive loading σ_0 shows that there is a non-dimensional loading parameter $\frac{\sigma_0}{\bar{E}}\left(\frac{a}{h}\right)^2$ where $\bar{E} = E/(1-\nu^2)$ and the length a is characteristic of the buckle equilibrium morphology (Parry et al., 2006). The length a can be the half-with b of a straight-sided blister or the radius R of a circular blister (Hutchinson and Suo, 1992a).

For these highly symmetric geometries the buckle edge is everywhere critical, *i.e.* the energy release rate is everywhere equal to the critical energy release rate. For TCs however, this is no longer the case. The morphology is defined by the propagation kinematics, and it may (and does) happen that this kinematics leaves behind portions of buckle edge where the energy release rate lies below the critical value. This is precisely the case for the so-called pinning point we identified earlier (Faou et al., 2012), where plate sagging develops strong mode II. As a result, approximations of the TC buckle morphology by models assuming critical loading all along the edges are prone to errors in estimating both the energy release rate and the phase angle. In contrast, for TCs our experiments and simulations point to the wavelength λ as the primary morphological parameter, in relation to adhesion. Rewriting Eq. 11 we obtain

$$\frac{\sigma_0}{E}\left(\frac{\lambda}{h}\right)^2 = \frac{k^2}{\sqrt{\frac{G_0}{G_{Ic}} - 1}} \tag{12}$$

The wavelength depends on the position of the pinning point (or sag) forming along the front of the buckle, which is controlled by the propagation

kinematics of the buckle, impacted by both plate response and adhesion.

For TCs, we conclude that it is the wavelength which directly depends on adhesion. For simpler buckles, it is the width $2b$. In many aspects, in TC buckles, the wavelength behaves differently from – even sometimes contrary to – the width. For instance, let us imagine a slight increase of adhesion while keeping other properties (material, stress, thickness) unchanged. For a straight-sided blister, increased adhesion would result in smaller width. However, for the TC blisters, following from Eqs. 11 or 12, stronger adhesion results in longer wavelength. In fact, this behavior is due to the narrower front (smaller width), which is more difficult to destabilize, delaying the formation of the pinning point. Conversely increasing the residual stress facilitates destabilization, resulting in smaller TC wavelength, while for a straight-sided buckle, it results in increased width.

6.2. Total elastic energy and energy release rate in TC buckles

It is somewhat unexpected that the normalized loading ratio involves the energy ratio G_0/G_{Ic} (Eq. 10) and not the energy release rate ratio $\overline{G}/G_{Ic}$.

To better understand this difference, we have calculated the average energy release rate $\overline{G}$ during propagation for several TC buckle morphologies and plotted $\overline{G}/G_0$ as a function of σ_0/σ_c in Fig. 9. We also plotted the results obtained by Moon et al. (2004) for the delamination of a straight-sided blister. Altogether $\overline{G} = 0.65 \pm 0.05\ G_0$, *i.e.* there is a very limited variation of $\overline{G}/G_0$ within the family of buckles we have investigated. This observation points to the fact that $\overline{G}/G_0$ is almost insensitive to both loading ratio and aspect ratio. Indeed Moon et al. (2004) commented that the maximum dependence of $\overline{G}/G_0$ on loading ratio is observed for $\sigma_0/\sigma_c < 20$: precisely the range where no TC buckle is observed experimentally or numerically! Note however that the average energy release rates found here (for full buckle kinematics) are lower by about 15% than Moon et al. (2004)'s values (for secondary buckling). Although these two varieties of TCs look alike, the exact morphologies differ. In fact, when going through the full kinematics, the film does not completely delaminate over the strip of width $2b$: it is still attached to the substrate close to the pinning points (Faou et al., 2012).

Because of the moderate variation of $\overline{G}/G_0$ within the TC buckle family, it is tempting to use $\overline{G}$ instead of G_0 in Eq. 11. We find that this is possible but less accurate in predicting the resulting wavelength.

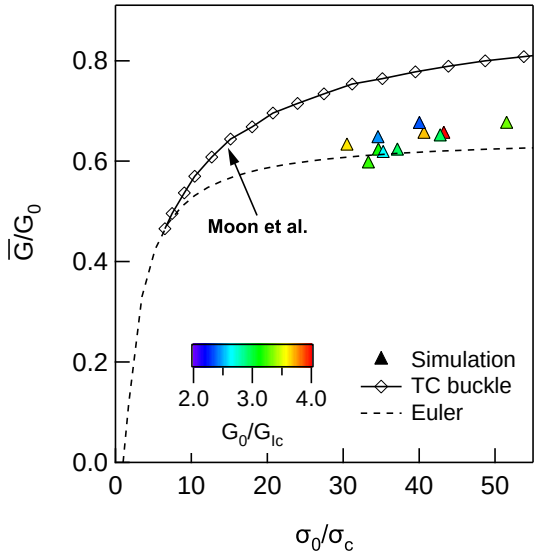

Figure 9: Average elastic energy release rate $\overline{G}/G_0$ as a function of loading ratio σ_0/σ_c, showing: 1) previous results for buckle delamination along a straight-sided strip, with straight sided (or Euler) blister (dashed line, valid for $\sigma_0/\sigma_c < 6.5$) and TC blister from secondary buckling (full line with markers, $\sigma_0/\sigma_c > 6.5$, from Moon et al. (2004)); 2) present results for full buckling driven delamination with mode dependent interfacial toughness (triangles, color coded for energy ratio).

6.3. Impact of mode II on wavelength

The linear relation Eq. 11 was obtained for the specific value $\eta = 0.95$. Changing the mode mixity dependence by varying η from 0.6 to 0.97, similar linear relations were found for λ as a function of loading, interface and material properties. It was found that the slope k decreases with η (Fig. 10). This variation is very slow however and k changes by only 10% when G_{IIc}/G_{Ic} drops from 450 to 2.9. We conclude that even though mode dependent interfacial toughness controls stability of the buckle edges and kinematics of buckle formation, the resulting wavelength is only weakly impacted by the mode II dependence. A possible reason is the range of mode mixity impacting TC buckle formation, which is quite remote from the limit mixity angle $-\pi/2$, where the maximum dependence of G_c upon mode mixity is found.

Note that η is not the only parameter influencing k. The cohesive tractions T_n^0 and T_t^0 defining the cohesive zone also impact k and a moderate increase of k was observed when the cohesive traction was increased. It is

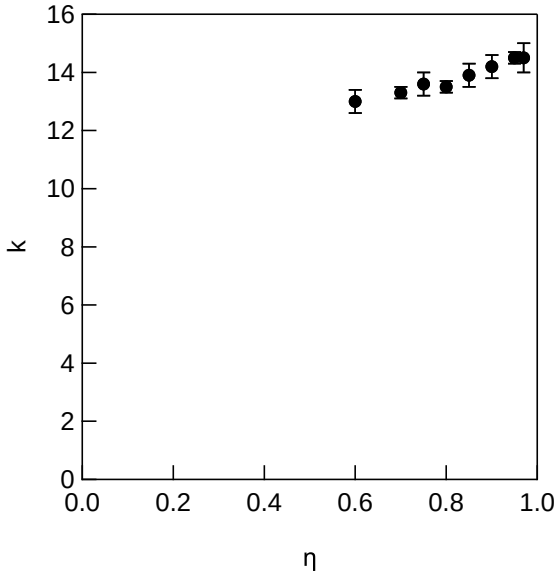

Figure 10: Computed prefactor k for the period of TC blisters as a function of the mode mixity parameter η.

expected that k converges to a finite value for large cohesive tractions. In addition, Eq. 4 is an idealized representation of the mode dependence of interfacial toughness. Real systems could possess a different dependence (Strohband and Dauskardt, 2003) also affecting the value of the k parameter. In brief, although our experimental value $k = 12.2$ lies close to the simulated values, we find it difficult to conclude on η and the mode mixity dependence based on this value.

7. Conclusion

We have studied the kinematics of formation of telephone cord buckles duly taking into account the details of film adhesion to the substrate, and especially the mode mixity dependence. Through extensive Finite Element Simulations, we have demonstrated that the aspect ratio $\lambda/2b$ of the telephone cord is rationalized if the loading ratio, defined from the buckle width $2b$, is normalized by a factor involving the energy ratio G_0/G_{Ic}. As a result, we find that it is the wavelength λ, and not the width, of the TC buckle which directly contains information about film adhesion, and a relation between λ and interfacial toughness in mode I G_{Ic} has been identified. Experiments have

also been carried out to confirm this relation, which has been tested against buckle morphology data. From the trends observed for various thicknesses and stresses, an estimate of the adhesion energy for an SiO_2/Ag interface has been inferred, which compares well with literature values.

8. Acknowledgements

We thank John Hutchinson for very useful discussions.

References

ABAQUS Manuals Collection, Dassault Systèmes Simulia Corp., Providence, RI, USA, 2010

Audoly B., Stability of straight delamination blisters, Phys. Rev. Let. 1999;83:4124

Audoly B., Roman B., Pocheau A., Secondary buckling patterns of a thin plate under in-plane compression, J. Eur. Phys. J. B 2002;27:7

Barthel E., On the description of the adhesive contact of spheres with arbitrary interaction potentials, J. of Colloid and Interface Sci. 1998;200:7

Barthel E., Kerjan O., Nael P., Nadaud N., Asymmetric silver to oxide adhesion in multilayers deposited on glass by sputtering, Thin Solid Films 2005;473:272-277

Cordill M. J., Bahr D. F., Moody N. R., Gerberich W. W., Adhesion measurements using telephone cord buckles, Mat. Sci. and Eng. A 2007;443:150-155

Evans A. G., Hutchinson J. W., On the mechanics of delamination and spalling in compressed films Int. J. Solids Structures 1984;20:455-466

Faou J.-Y., Parry G., Grachev S., Barthel E., How does adhesion induce the formation of telephone cord buckles?, Phys. Rev. Let. 2012;108:116102

Faou J.-Y., Barthel E., Grachev S. Y., Stress tuning in sputter-deposited MoOx films, Thin Solid Films 2013;527:222-226

Gilles G., Rau B., Buckling instability and adhesion of carbon layers, Thin Solid Films 1984;109-121

Gioia G., Ortiz M., Determination of thin-film debonding parameters from telephone-cord measurements, Acta materialia 1998;46;169-175

Hutchinson J. W., Delamination of compressed films on curved substrates J. Mech. Phys. Sol. 2001;49:1847-1864

Hutchinson J. W., Suo Z., Mixed mode cracking in layered materials, Adv. Appl. Mech. 1992;29:63-191

Hutchinson J. W., Thouless M. D., Liniger E. G., Growth and configurational stability of circular, buckling-driven film delaminations, Acta metall. mater. 1992;40:295-308

Jensen H. M., Energy release rates and stability of straight-sided, thin-film delaminations, Acta. metall. mater. 1993;41:601-607

Lee A., Litteken C. S., Dauskardt R. H., Nix W. D., Comparison of the telephone cord delamination method for measuring interfacial adhesion with the four-point bending method, Acta. mater. 2005;53:609-616

Liechti K. M., Chai Y. S., Asymmetric shielding in interfacial fracture under in-plane shear, J. App. Mech. 1992;59:295-304

Moon M.-W., Chung J.-W., Lee K.-R., Oh K. H., Wang R., An experimental study of the influence of imperfections on the buckling of compressed thin films, Acta. Mater. 2002;50:1219-1227

Moon M. W., Jensen H. M., Hutchinson J. W., Oh K. H., Evans A. G., The characterization of telephone cord buckling of compressed thin flms on substrates, J. Mech. Phys. Sol. 2002;50:2355-2377

Moon M.-W., Lee K.-R., Oh K. H., Hutchinson. J. W., Buckle delamination on patterned substrates, Acta Mater. 2004;52:3151-3159

G. Parry G., Cimetiere A., Coupeau C., Colin J., Grilhe J., Stability diagram of unilateral buckling patterns of strip-delaminated films, Phys. Rev. E 2006;74:066601

Patinet S., Alzate L., Barthel E., Dalmas D., Vandembroucq D., Lazarus V., Finite size effects on crack front pinning at heterogeneous planar interfaces: Experimental,finite elements and perturbation approaches, J. Mech. Phys. Sol. 2013;61:311-324

Strohband S., Dauskardt R. H., Interface separation in residually-stressed thin-film structures, Interface Sci. 2003;11(3):309-317

Thouless M. D., Combined buckling and cracking of films, J. Am. Ceram. Tech. 1993;76:2936-2938

Tvergaard V. and Hutchinson J. W., The relation between crack growth resistance and fracture process parameters in elastic-plastic solids, J. Mech. Phys. Solids 1992;40:1377-1397

Wang J. S., Evans A. G., Effects of strain cycling on buckling, cracking and spalling of a thermally grown alumina on a nickel-based bond coat, Acta. Metall. 1999;47:699-710

Xu X. P., Needleman A., Void nucleation by inclusion debonding in a crystal matrix, Model. Simul. Mater. Sci. Eng. 1993;1:111-132

Yu S.-J., Chen M.-G., Chen J., Zhou H., Zhang Y.-J., Si P.-Z., Spatial and kinetic evolutions of telephone cord buckles, Surf. Coat. Tech. 2013;228:258-265